Published in final edited form as:
J Phys Chem C Nanomater Interfaces. 2008 July 24; 112(29): 10721–10724. doi:10.1021/jp801684j.

Zinc Oxide Nanocrystals for Non-resonant Nonlinear Optical Microscopy in Biology and Medicine

Aliaksandr V. Kachynski, **Andrey N. Kuzmin**, **Marcin Nyk**, **Indrajit Roy**, and **Paras N. Prasad***
The Institute for Lasers, Photonics, and Biophotonics, University at Buffalo, The State University of New York, Buffalo, NY 14260, USA

Abstract

In this paper we show that biocompatible zinc oxide (ZnO) nanocrystals (NCs) having non-centrosymmetric structure can be used as non-resonant nonlinear optical probes for targeting in bioimaging applications *in vitro* by use of the second order processes of second harmonic and sum frequency generation, as well as the third order process of four wave mixing. These non-resonant processes provide advantages above and beyond traditional two-photon bioimaging: (i) the probes do not photo-bleach; (ii) the input wavelength can be judiciously selected; and (iii) no heat is dissipated into the cells, ensuring longer cell viability and ultimately longer imaging times. ZnO NCs have been synthesized in organic media by using a non-hydrolytic sol-gel process, and subsequently dispersed in aqueous media using phospholipid micelles, and incorporated with the biotargeting molecule folic acid (FA). Sum Frequency, Second Harmonic and non-resonant four wave mixing non-linear signals from this stable dispersion of ZnO NCs, targeted to the live tumor (KB) cells were used for imaging. Robust intracellular accumulation of the targeted (FA incorporated) ZnO nanocrystals could be observed, without any indication of cytotoxicity.

Introduction

Nonlinear optical microscopy is emerging as a valuable imaging tool for both *in-vitro* and *in-vivo* biomedical applications. A number of nonlinear optical processes such as two- (or multi-) Photon Excited Fluorescence (TPEF), second and third harmonic generation (SHG and THG), and vibration coherent anti-Stokes Raman scattering (CARS) have been used for live cells and tissue imaging [1–3]. These processes offer a number of advantages over other linear optical techniques. The nonlinear nature of interaction (quadratic or higher order dependence of the response on the intensity of light) produces a high 3D spatial resolution and improved signal to noise ratio. The imaging depth is also increased by use of near IR laser wavelengths, which can be selected to be in the biological window of maximum optical transparency. Ultra short laser pulse durations reduce the thermal interaction and stress for the biological specimen. The most commonly used nonlinear optical process in bioimaging is two-photon excited fluorescence [1], which is a resonant process. However, it requires an efficient two-photon excitation limited to a specific wavelength, which corresponds to two-photon resonance of the dye. In addition, because of its resonant nature, the dye is susceptible to photobleaching. Furthermore, for targeted imaging one has to rely either on the natural targeting abilities of the dye, or chemically conjugate it to a targeting moiety. In this regard, non-resonant non-linear processes may offer new advantages due to a total absence of light absorption of the stained material, which makes them free from photobleaching and thermal interaction, and due to narrow spectral line of the incoming and outgoing emission. Unfortunately, the use of second order processes has been limited as, in general, the centrally symmetrical structure of cell

*Corresponding author. E-mail: E-mail: pnprasad@acsu.buffalo.edu.

component materials, which results in a small output of SHG from the interface layers, low contrast, and image quality [4]. As for third-order processes, although Coherent Anti-Stokes Raman Scattering is receiving considerable attention for bioimaging [3], to our knowledge there is no report of bioimaging using non-resonant electronic four-wave mixing primarily due to low magnitude of $\chi^{(3)}$ third order nonlinear susceptibility of cellular components.

One of the promising nontoxic and biocompatible semiconductor materials for nanoparticle design is zinc oxide (ZnO) [5], which has already found widespread applications as a UV-blocker for skin protection gels and creams. The excitation of pure and doped ZnO optical fluorescence lies in the UV and blue wavelength range [5], which is not convenient for imaging of cells and biological tissue. On the other hand, ZnO nanocrystals possess large second-order and third-order non-linearities [5–7] resulting in the production of SHG, SFG and electronic Four–Wave Mixing (FWM), which could be successfully applied for biological microscopy. Preparation of a uniform, isotropic water dispersion of well separated single nanocrystals is one of the important conditions needed for high quality imaging by using labeling technology. The phospholipid micelles (a.k.a. diacyllipid micelles or polymeric micelles), formed by the self-assembly of polymer-grafted lipids such as poly(ethyleneglycol)-phosphoethanolamine (PEG-PE) in aqueous system, have been used extensively for encapsulating a variety of mostly water insoluble agents, ranging from small molecule drugs to nanosized materials like quantum dots [8,9]. Such micelles are uniquely suited for biomedical applications such as drug delivery, owing to their extremely low critical micelle concentration (CMC), high aqueous stability, the presence of an external layer of PEG rendering them with the ability for prolonged systemic circulation, and the easy incorporation of biotargeting molecules for site-specific delivery [8–10]. Our group has also shown the ability to co-encapsulate magnetic nanoparticles and photosensitizer drugs within these micelles, for the purpose of magnetically guided drug delivery in photodynamic therapy [11].

In this article, we have used successful encapsulation of ZnO nanocrystals, being initially synthesized in organic media by using a non-hydrolytic sol-gel process, within the non-polar core of phospholipid micelles, with and without the incorporated tumor-avid molecule folic acid (FA) for nonlinear SHG, SFG and FWM imaging. The micelle-encapsulated ZnO nanocrystals are highly stable and retain their non-linear optical properties in aqueous dispersion. For *in vitro* studies, KB (human nasopharyngeal epidermal carcinoma) cells were used, which are known to overexpress receptors for folic acid [12]. Using SFG and SHG imaging from live KB cells treated with nanoparticles, it was observed that while the intracellular uptake of the non-targeted ZnO nanocrystals is rather week, robust intracellular signal could be generated from the cells treated with targeted (FA incorporated) ZnO nanocrystals. No indication of cytotoxicity could be observed at the experimental dosages. To the best of our knowledge, this is the first report utilizing ZnO nanocrystals as targeted nonlinear optical probes for bioimaging.

Synthesis of ZnO nanoparticles

Zinc acetate dihydrate (98+% Aldrich), benzyl ether (99% Aldrich), trioctylphospine oxide (TOPO, 90% Aldrich), n-tetradecylphosphonic acid (TDPA, 97% Alfa Aesar), 1,2-dodecanediol (90% Aldrich), 11-mercapto-undecanoic acid (MUA, 95% Aldrich), sodium hydroxide pellets (J.T. Baker). Distearoyl-Phosphoethanolamine-methoxy-polyethyleneglycol-2000 (DSPE-PEG2000) and Distearoyl-Phosphoethanolamine-folate-polyethyleneglycol-2000 (DSPE-PEG2000-FA) were purchased from Avanti Polar Lipids. KB (human nasopharyngeal epidermal carcinoma) cells were obtained from ATCC. All other cell culture reagents were obtained from Invitrogen.

ZnO nanocrystals were synthesized by using a non-hydrolytic sol-gel process as proposed by Joo et al. [13] and is based on the ester-elimination reaction between zinc acetate and 1,2-dodecanediol. In our case, benzyl ether was selected as the solvent, with its high boiling point to increase the synthesis temperature to 280°C, which stabilizes the synthesis so that it provides high-quality samples with excellent size control, narrow size distribution, good crystalline morphology and dispersive properties. A High (10 mM) molar concentration of Zn acetate in then dehydrated resulting in supersaturation of the solution which increases the yield of reaction.

Brifely, 10 mM zinc acetate and 6 mM TOPO were added to a three-neck flask using 15 ml benzyl ether as a solvent. The resulting solution was slowly heated to 200 °C under vacuum with magnetic stirring for 15 min to remove residual water during which time the flask was purged periodically with dry argon gas. Then the solution mixture was kept at 200 °C for 1 h with vigorous stirring. The resulting solution was cooled to ~50 °C and 10 mmol of 1,2-dodecanediol was added. In the next step, the mixture was heated for a second time under Ar to 280 °C and stirred for 2h. Finally, ethanol was added to increase precipitation of ZnO NC; which were collected by centrifuging at 11000 rpm for 30 min, then washed with ethanol once, and dried in a vacuum oven at room temperature.

The characterization of the size and the morphology of the nanocrystals were performed by using the transmission electron microscopy (TEM) and by X-ray diffraction (XRD). ZnO nanocrystals with a dimension less than 100 nm were shaped as trigonal pyramids as shown by the TEM picture in Fig. 1. The crystal structure of the non-centrosymmetric ZnO nanocrystals was identified by the XRD spectrum (Fig. 2), which corresponds to the hexagonal wurtzite unit cell.

Finally, ZnO nanocrystals were stably dispersed in distilled water using phospholipid micelles as the stabilizer. The phospholipid micelles are comprised of DSPE-PEG-2000 and DSPE-PEG2000-FA (Avanti Polar Lipids). Briefly, 100 μL of ZnO nanocrystals in chloroform (17 mg/mL) was mixed either with (a) 500 μL of DSPE-PEG2000 (20 mg/mL in chloroform), or (b) a mixture of 480 ul of DSPE-PEG (20 mg/mL in chloroform) and 200 μL of DSPE-PEG2000-FA (2 mg/mL chloroform). Then chloroform was evaporated using a rotary vacuum evaporator and the dry film was dispersed in 3 ml of distilled water by vortexing. The aqueous dispersion of ZnO nanocrystals was then sterile filtered prior to treatment with cells in culture.

Experimental setup, results and discussion

The experimental set-up is schematically shown in Fig. 3. Picosecond diode pumped Nd:YVO_4 laser (*Laser 1* in Fig. 3), *picoTRAIN IC-10000 1064nm* (HighQ Laser) with the pulse width ~10 ps and a repetition rate of 76MHz was used both as a source for ν_1 incident wave. It also was used for synchronous pumping of *Laser 2* - a tunable (781–923 nm) optical parametric oscillator *Levante* (APE) to produce another incident wave ν_2 of ~10 ps pulse duration. *Laser 1* and *Laser 2* have been used separately for SHG signal generation at the sample. SFG and FWM signal generation require coherent mixing of ν_1 and ν_2 incident waves. For the coherent mixing process computer controlled delay line provided the temporal synchronization of picosecond pulses of the Nd:YVO_4 laser and the OPO with a zero time jitter, and adjustable telescopes T1 and T2 ensured the beams focal point conjugation at the plane of the microscope specimen. Picosecond outputs of *Laser 1* and *Laser 2*, coinciding in time and in space were directed to an inverted microscope *TE2000-S* (Nikon). A computer-controlled XY galvano scanner *VM1000* (GSI Lumonics) insured fast laser beams scan along the sample in the lateral (XY) focal plane of the water-immersion objective *O1, UPLSAPO 60XW*, NA=1.2 (Olympus). The objective *O1* was mounted on a computer-controlled piezo-stage (Piezosystem Jena) for an axial laser beam Z-scanning through the sample, with the

minimum step of 0.1 nm. Splitting power ratio of *Laser1* output between the pump power of *Laser2* and the ν_1 incident wave was controlled by the half-wave ($\lambda/2$) waveplate *WP1*. Polarizations of *Laser 1* and *Laser 2* were computer-controlled by rotating Glan-Thomson polarizers *P1* and *P2* and half-wave plate WP2. The SHG/SFG signals generated in the specimen plane were detected by a photomultiplier tube R928 (Hamamatsu Photonics), PMT1, in the reflection geometry; the narrow-bandpass barrier filter *F1* cuts the fundamental frequencies ν_1 and ν_2 and separate $2\nu_1/2\nu_2$ (SHG) or $\nu_1 + \nu_2$ (SFG) signals. The nonlinear FWM response at the frequency $2\nu_2 - \nu_1$, generated by ZnO nanocrystals dispersion in forward direction, spectrally separated from ν_1 and ν_2 by a dichroic mirror, M11, and a barrier filter, F2, was detected by a photomultiplier tube R5108 (Hamamatsu Photonics), PMT2. A consistent operation of the optical scanner and acquisition system ensures digitization of the nonlinear signal at new frequencies $2\nu_1$, $2\nu_2$, $(\nu_1+\nu_2)$ and $(2\nu_2 - \nu_1)$ and generates the nonlinear optical images.

Human nasopharyngeal epidermal carcinoma (KB) cells were chosen for imaging. The cell culture was plated overnight in 35 mm glass bottom cell dishes in a minimum essential medium (MEMα). with 10 % FBS and appropriate antibiotic, according to the manufacturers instructions (American Type Culture Collection). Next day, with the cells at a confluency of 70 %, the overnight media was aspirated and replaced with a fresh medium (2 mL/dish). To study the uptake, 200 μL of the aqueous dispersion of the ZnO nanoparticles (with and without incorporated folic acid) were added, mixed by gentle swirling, and replaced in the incubator at 37°C with, 5% CO_2 (VWR Scientific, 2400). After 1 and 3 hours of incubation, the cells were rinsed with PBS and directly imaged.

In general, the light induced nonlinear polarization for a medium can be expressed by [14]:

$$\boldsymbol{P}=\chi^{(1)}\boldsymbol{E}^{\mathbf{1}}+\chi^{(2)}\boldsymbol{E}^{\mathbf{2}}+\chi^{(\mathbf{3})}\boldsymbol{E}^{3}+\ldots,$$

where $\boldsymbol{P}$ is the induced polarization, $\chi^{(n)}$ is the n^{th} order of nonlinear susceptibility, and $\boldsymbol{E}$ is the electric field vector of the incident light. The first term, $\chi^{(1)}\boldsymbol{E}^{\boldsymbol{1}}$, describes normal absorption and reflection of light, the second term , $\chi^{(2)}\boldsymbol{E}^{\boldsymbol{2}}$, describes SHG, SFG, and difference frequency generation, and the third term, $\chi^{(3)}\boldsymbol{E}^{\boldsymbol{3}}$, describes THG and TPEF, as well as FWM, including vibrational Coherent anti-Stokes Raman Scattering. In this article we present a demonstration of successful application of the second order SHG and SFG, and the third order FWM nonlinear phenomena in an aqueous dispersion of phospholipid micelle-encapsulated ZnO single nanocrystals for cellular bioimaging.

For nonlinear spectroscopy of ZnO nanocrystals, a sealed aqueous suspension of ZnO nanoparticles (~0.3% wt) between a glass slide and a cover slip sealed by *Eppendorf* in situ Frame* was used as a specimen. Two laser beams with required combinations of the laser frequencies ν_1 and/or ν^2 were introduced into the microscope. *Laser 1* and *Laser 2* were adjusted to approximately equal average power of 150 mW at the frequencies ν_1 and ν_2 in the focal plane of microscope objective *O1*. Computer controlled laser shutters and tunable OPO wavelength varied the combination of the frequencies at the specimen. Nonlinear signals, generated by ZnO nanoparticles suspension, were picked up on the location of detectors PMT1 and PMT2 by the input fiber of the spectrometer *SpectraPro® 2500i* (Acton Research) equipped with *Spec-10:100B* CCD (Princeton Instruments). Four types of nonlinear optical response of ZnO nanocrystals were detected by the spectrometer. The experimental data for the combination of incident wavelength λ_1 = 1064 nm and λ_2 = 850.6 nm are presented in Fig. 4. Narrow linewidth high efficient second harmonic output at 532 nm ($2\nu_1$) from *Laser 1* (Fig. 4a) and at 425.3 nm ($2\nu_2$) from *Laser 2* (Fig. 4b) were derived from the sample when the laser shutters were opened alternatively for *Laser 1* or *Laser 2*. High intensive narrow line SFG

signal at 472.7 nm ($\nu_1 + \nu_2$) was detected in the backward propagating direction (Fig. 4c) and FWM signal at 708.5 nm ($2\nu^2 - \nu_1$) was detected in the forward direction (Fig. 4d) when both shutters were opened. The second order susceptibility $\chi^{(2)}$ characterizes the first three new wavelengths of SHG (532 nm, 425.3nm) and SFG (472.7 nm) output intensity emissions. The FWM intensity signal at 708.5 nm is characterized by the third order susceptibility $\chi^{(3)}$ of ZnO nanocrystals. To compare the efficiency of these nonlinear outputs, a square area of the ZnO nanoparticles homogeneous suspension was scanned and the average image intensity for SHG, SFG and FWM was measured. The experimental signal intensities are shown in the Table 1. It is noteworthy, that all four new generated signals are intense enough to generate microscopy images. Moreover, the SFG/SHG output (SHG and SFG were not separated) is about twice higher than that of SHG when both laser shutters were opened and laser pulses were delayed in time for ~ 5 ps. Thus, SFG signal from ZnO nanoparticles can provide an opportunity for high contrast bioimaging by tuning on both beams through the near IR spectral region of maximum biological transparency.

The confocal SFG images of KB cells treated with the aqueous dispersion of ZnO and ZnO-FA (targeted by folic acid), for 1 and 3 hours, are shown in Fig. 5a–d. It can be seen that while for the non-targeted ZnO the intracellular uptake is poor in the case of, 1 and 3 hours of treatment (Fig. 5a, b), robust intracellular SFG signal is observed in the case of cells treated with ZnO-FA for 3 hours (Fig. 5d). The nanoparticles seem to be distributed throughout the cytoplasm. The localized narrow spectrum, a laser like line, confirms the observed SFG from internalized nanoparticles. Besides SFG response, intensive FWM output was generated by ZnO nanoparticles in the forward direction of the incident beams. The corresponding images of FWM and SFG signals in the same scan are shown in Fig. 5e and Fig. 5f. We could clearly identify FWM emission (arrows in Fig. 5, e) exactly from the same location where SFG signal was detected (arrows in Fig. 5, f). However, in contrast to the SFG signals generated by ZnO nanoparticles, the FWM nonlinear response is generated both by internalized nanoparticles and cell compartment materials such as lipids, membranes, proteins, etc. This reduces the contrast of FWM imaging of ZnO nanocrystals and favors SFG for bioimaging application. To the best of our knowledge, this experiment is the first demonstration of targeted intracellular delivery of ZnO nanocrystals and of non-linear optical bioimaging using these nanoparticles. During our experiments with the maximum laser peak intensity of ~ 6 GW/cm^2, scanning speed of ~ 0.1 m/sec and scanned area ~ 70 ×70 μm^2, there was no evidence of photodamage of the cells found even after 50 sequential image scans. Using a cell viability (MTS) assay, no indication of cytotoxicity could be observed at the experimental dosage (data not shown), thus further highlighting the potential of ZnO nanocrystals as non-toxic nonlinear optical probes for diagnostic imaging.

Conclusion

In conclusion, we have demonstrated the use of photostable water-dispersible ZnO nanoparticles for high contrast non-resonant nonlinear optical bioimaging. The photostable ZnO nanoparticles were dispersed in water using phospholipid micelles. The micelles act not only as stabilizers of the nanoparticles in physiological conditions, but also render them with the capability of site-specific delivery, using incorporated biotargeting molecules such as folic acid (FA). Using SFG microscopy, we have demonstrated a robust internalization of ZnO-FA nanoparticles in human nasopharyngeal epidermal carcinoma (KB) cells. The usage of two picosecond beams with ν^1 and ν^2 frequencies for SFG imaging improves the signal contrast and essentially extends the potential of multi-channel microscopy by combining a number of advanced nonlinear optics approaches such as CARS, TPEF, cell generated SHG and THG, to obtain extended cellular information in the same scan. Therefore, this promising, nontoxic, and biocompatible nanomaterial demonstrates their potential as a nonlinear optical probe for diagnostic imaging. The effect of successful internalization of ZnO-FA nanoparticles in live

cells to generate *in situ* new frequency components can be promising for photo-chemical interactions inside the cells, such as photodynamic therapy. Further development of these nanocrystals for advanced applications, such as *in vivo* bioimaging and photodynamic therapy, are underway.

ACKNOWLEDGMENT

This work was supported in part by NIH grants CA119397 and CA104492, and the John R. Oishei Foundation. Partial support from the center of Excellence in Bioinformatics and Life Sciences at University at Buffalo is also acknowledged. The authors also thank Adela C. Bonoiu for assistance with cell viability assay studies.

REFERENCES

1. Prasad, PN. Introduction to Biophotonics. New York: John Wiley & Sons; 2003.
2. Squier J, Muller M. Rev. Sci. Instrum 2001;72:2855–2867.
3. Cheng J-X, Xie XS. J. Phys. Chem. B 2004;108:827–840.
4. Campagnola PJ, Clark HA, Monler WA, Lewis A, Loew LM. J. Biomedical Optics 2001;6:277–286.
5. Djurišić AB, Leung YH. Small 2006;2:944–961. [PubMed: 17193149]
6. Larciprete MC, Passeri D, Michelloti F, Paoloni S, Sibilia C, Bertolotti M, Belardini A, Sarto F, Somma F, Lo Mastro S. J. Appl. Phys 2005;97:023501.
7. Johnson JC, Yan H, Schaller RD, Petersen PB, Yang P, Saykally RJ. Nano Lett 2002;2:279–283.
8. Torchillin VP, Lukyanov AN, Gao Z, Papahadjopoulos-Sternberg B. Proc. Natl. Acad. Sci. U.S.A 2003;100:6039–6044. [PubMed: 12716967]
9. Dubertret B, Skourides P, Norris DJ, Noireaux V, Brivanlou AH, Libchaber A. Science 2002;298:1759–1762. [PubMed: 12459582]
10. Lukyanov AN, Torchillin VP. Adv. Drug Deliv. Rev 2004;56:1273–1289. [PubMed: 15109769]
11. Cinteza LO, Ohulchanskyy TY, Sahoo Y, Bergey EJ, Pandey RK, Prasad PN. Mol. Pharm 2006;3:415–423. [PubMed: 16889435]
12. Bharali DJ, Lucey DW, Jayakumar H, Pudavar HE, Prasad PN. J. Am. Chem. Soc 2005;127:11364–11371. [PubMed: 16089466]
13. Joo J, Kwon SG, Yu JH, Hyeon T. Adv. Mater 2005;17:1873–1877.
14. Prasad, PN.; Williams, DJ. Introduction to Nonlinear Optical Effects in Molecules and Polymers. John Wiley & Sons; 1991.

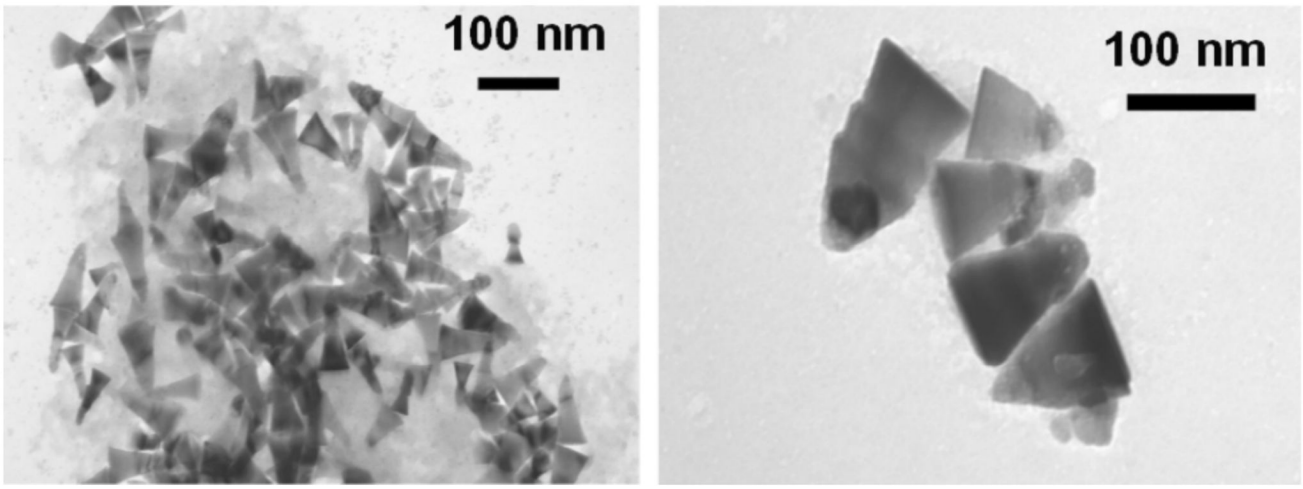

Figure 1.
TEM Images of ZnO Nanocrystals.

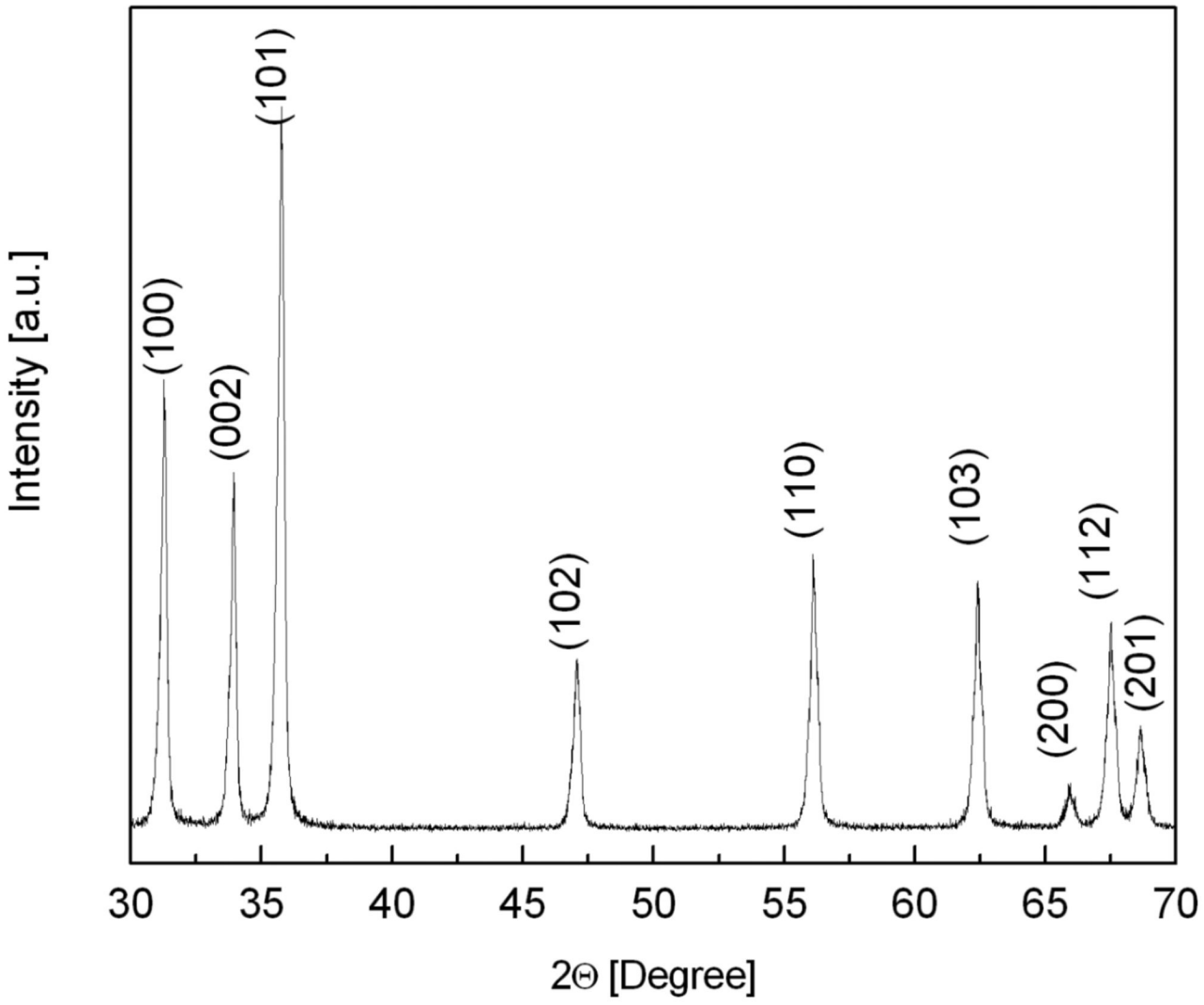

Figure 2.
X-Ray Diffarction Pattern of ZnO nanocrystals.

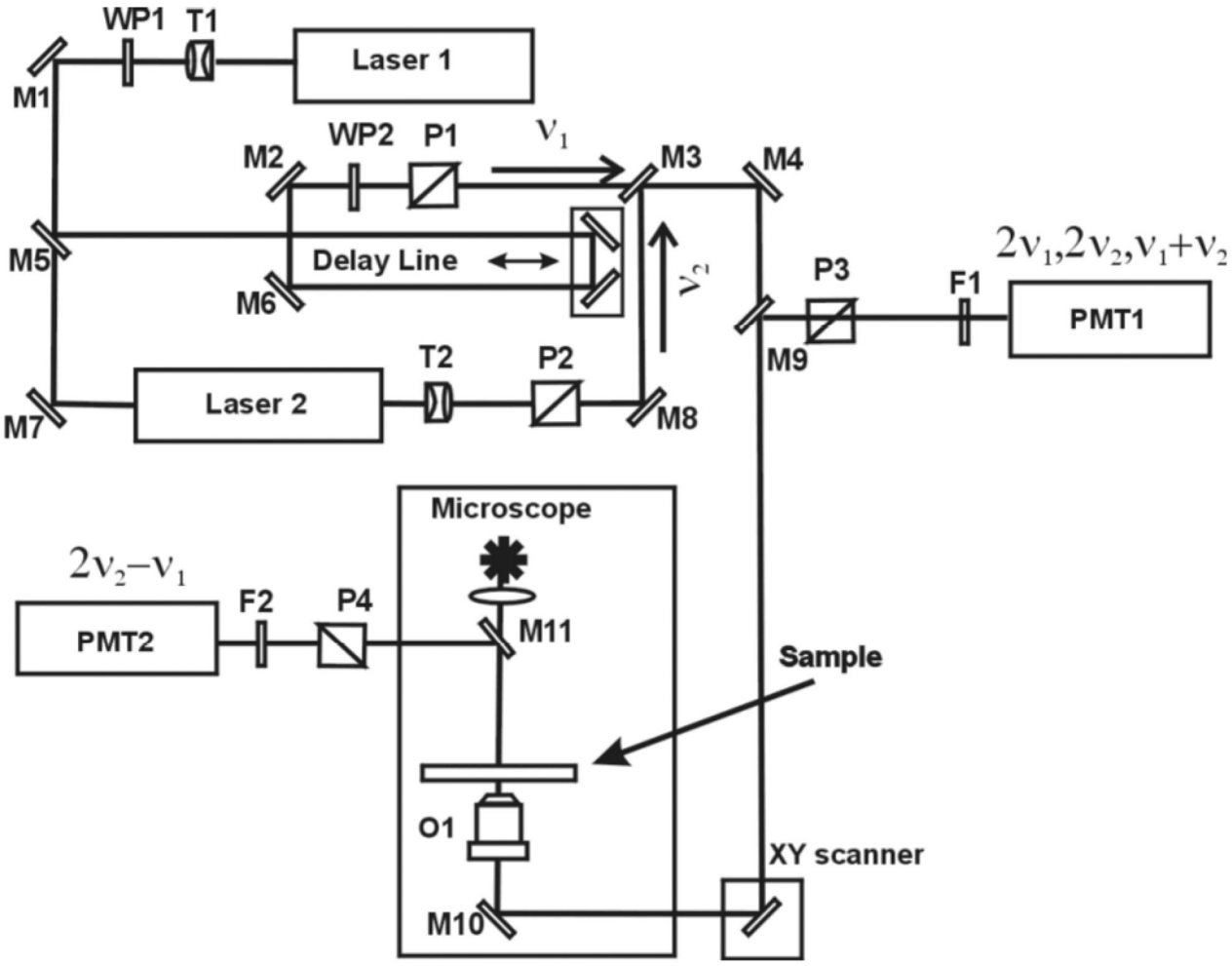

Figure 3.

Optical setup of the laser scanning SHG/SFG imaging system. *Laser 1* and *Laser 2* are picosecond lasers with the outputs at ν^1 and ν^2, respectively; *T1* and *T2* are lens telescopes; *WP1* and *WP2* –λ/2 waveplates; *M1 – M10* are dichroic dielectric mirrors; *O1* is objective lens; *PMT1*, *PMT2* are photomultiplier tubes. The optical *Delay Line*, the barrier filter wheels, *F1* and *F2*, the Glan-Thompson polarizers, *P1 – P4*, and the galvano *XY scanner* are all controlled by a computer.

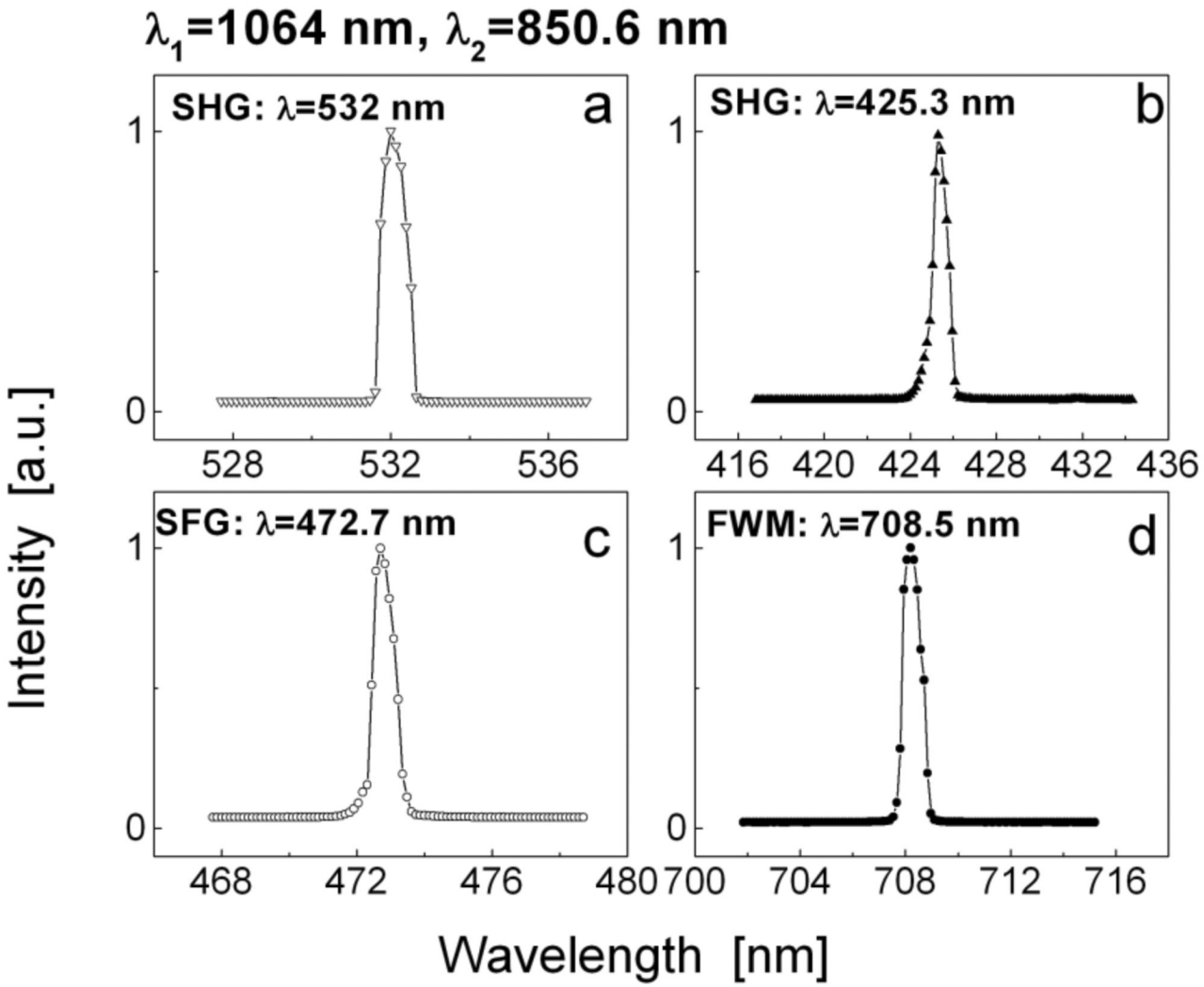

Figure 4.
Spectral distribution of SHG (a, b), SFG (c), and FWM (d) signals generated by the water-dispersed ZnO nanocrystals (λ_1 = 1064 nm and λ_2 = 850.6 nm).

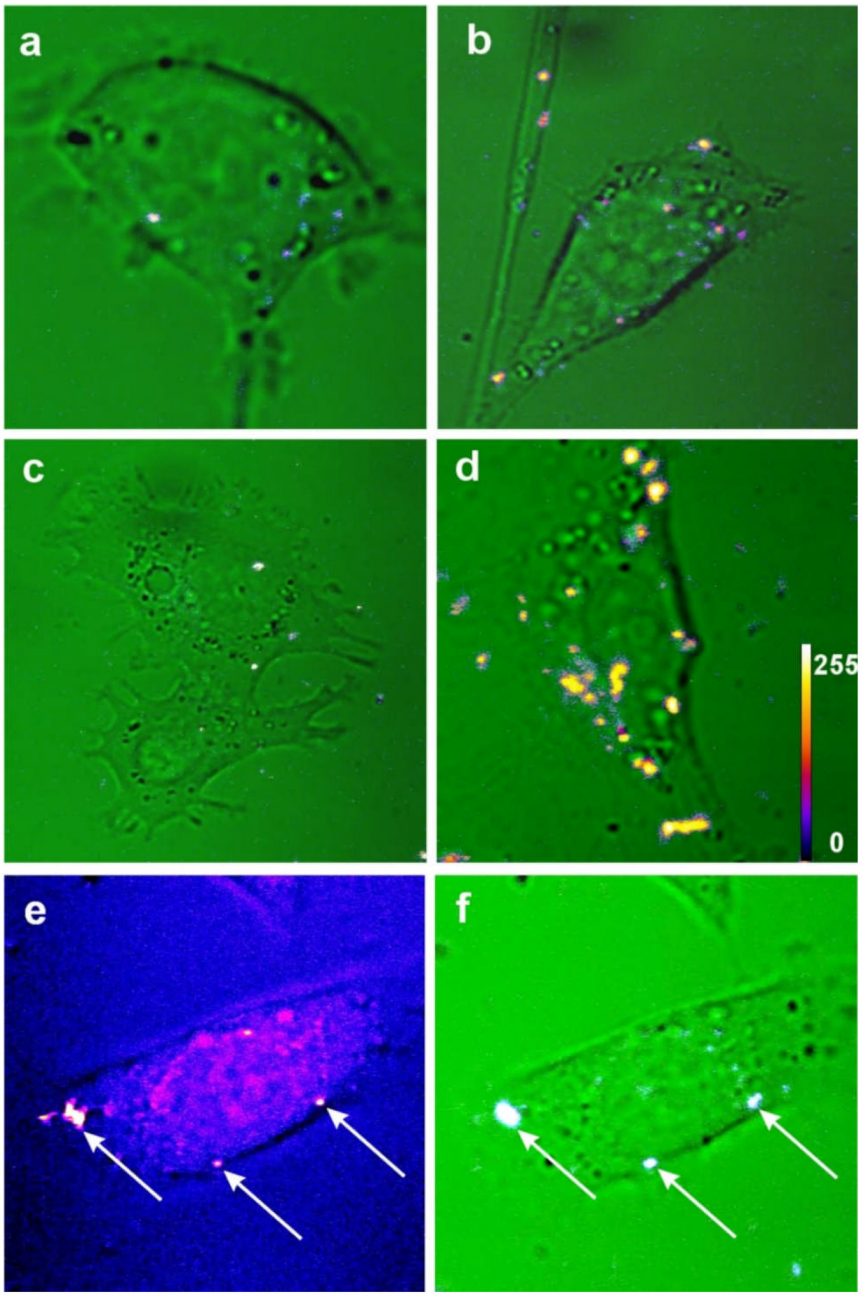

Figure 5.
The SFG and FWM nonlinear optical images of treated KB cells. The SFG images of KB cells treated by the ZnO nanoparticles non-targeted (a,c) and targeted with folic acid (b,d), after 1 (a,b) and 3 (c,d) hours of incubation. The intensity-coded SFG images (see scale inset on panel d) were superimposed on the transmission 1064 nm green color background images. (e) FWM image without transmission background and (f) is the corresponding SFG image of KB cells.

TABLE 1

Signal intensity distribution for SHG/SFG and FWM output.

Laser Shutters Status		**SHG/SFG output intensity at 532 nm, 425.3 nm, 472.7 nm, a.u.**	**FWM output intensity at 708.5 nm, a.u**
Laser 1	***Laser 2***		
On	Off	4800	-
Off	On	5300	-
On	On	13000	12000
On/Delayed	On	7000	-